Rev.Adv.Mater.Sci. 25 (2010) 23-31

MULTISCALE MODELLING OF BACK-STRESS DURING EQUAL-CHANNEL ANGULAR PRESSING

Enze Chen[1], Laurent Duchêne[2], Anne-Marie Habraken[2] and Bert Verlinden[1]

[1]Katholieke Universiteit Leuven, Department of Metallurgy and Materials Engineering, Kasteelpark Arenberg 44, B3001 Heverlee, Belgium
[2]FNRS Fonds de la Recherche Scientifique, University of Liège, Departement ARGENCO, Chemin des Chevreuils 1, B-4000 Liège, Belgium

Received: November 27, 2009

Abstract. Equal-channel angular pressing (ECAP) is a well known process to produce ultrafine-grained materials. The mechanical properties of these materials, including a compression-tension asymmetry and a transient hardening saturation in the beginning of the flow curve, largely depend on the evolution of the microstructure during ECAP. Consequently, the back-stress induced by the dislocation microstructure exhibits kinematic hardening at the macroscopic scale. In this paper, commercial purity aluminium AA1050 is processed by ECAP route C. Tensile and compression specimens are machined from the post-ECAP samples. The back-stress level is estimated from the different yielding strengths of tensile tests and compression tests. Then two different models, a macroscopic phenomenological Teodosiu-type model and a microscopic dislocation-based multi-layer model, are used to predict the back-stress values. A set of parameters for Teodosiu's model is identified from simple shear tests, Bauschinger tests and orthogonal tests. The dislocation-based multi-layer model is based on the Estrin-Tóth dislocation model and Sauzay's intragranular back-stress model. The predicted and experimental back-stresses due to ECAP are compared and critically evaluated.

1. INTRODUCTION

The Equal Channel Angular Pressing (ECAP) process can impose very large strain upon a material to generate an ultra-fine grained microstructure [1]. It has been found that these ECAP processed materials exhibit significant kinematic hardening during mechanical tests, e.g. the tension-compression asymmetry [2]. This phenomenon results from the existence of back-stress induced by the dislocation cell-and-wall microstructure, which is introduced into the material during ECAP processing.

The aim of the present paper is to model the back-stress evolution during ECAP and predict the back-stress level after ECAP. A macroscopic phenomenological hardening model from Teodosiu and Hu [3,4] is investigated first. This model is able to describe both the kinematic and isotropic hardening. In addition, a new dislocation-based mixed-hardening model is proposed, based on the Estrin-Tóth hardening model [5] and Sauzay's back-stress model [6]. Thanks to Sauzay's work, the present model is able to describe the back-stress evolution,

Corresponding author: Enze Chen, e-mail: enze.chen@mtm.kuleuven.be

which changes the isotropic Estrin-Tóth model into a mixed-hardening model.

The paper is organized in the following way. In Section 2, the experimental methods used to estimate the back-stress are explained and the results are shown. The simulation using the Teodosiu-Hu model is performed and investigated in Section 3. The new dislocation-based mixed-hardening model is proposed and its theoretic prediction is given in Section 4. A comparison of these two models and their results are discussed in Section 5. Finally, the main findings of this work are summarized in the conclusion.

2. EXPERIMENTAL METHODS AND RESULTS

2.1. ECAP processing

The ECAP die is mounted on a hydraulic press with a maximum force up to 110 kN. The used die is shown in Fig. 1a. The diameter of the ingoing channel is 12.1 mm and the outlet channel diameter is 11.7 mm. The slightly reduced diameter not only facilitates re-inserting the sample in the following ECAP pass, but also permits a better die filling-up condition when the material meets the bottom corner of the die. This ensures a more homogeneous material after ECAP processing. The channel angle Φ is 90° and the additional angle Ψ, which represents the arc of the curvature where the two parts of the channel intersect, is 0°. According to the work from Iwahashi *et al.* [7], the imposed shear strain r after each pass is equal to 2 and the equivalent strain is around 1.15. In order to mathematically describe the deformation, a global reference frame is established by right-handed convention. Axis 1 represents the Extrusion Direction (ED), Axis 2 is parallel with the Ingoing Direction (ID) and Axis 3 represents the Transverse Direction (TD) (Fig. 1b).

The experimental material is cut from a hot-rolled plate of commercial purity aluminium AA1050. The chemical composition of this plate is shown in Table 1. Its initial mean grain size was 29 μm (measured by electron backscattered diffraction (EBSD) in the ND–RD section). The Orientation Distribution Function characterizing the texture is measured by a Siemens D500 goniometer and the texture is discretized into a set of 2000 representative crystals. The specimen is machined from this plate along the rolling direction. It has a cylindrical shape with a diameter of 11.9 mm and a length of 60 mm.

The ECAP process is performed up to 8 passes at room temperature. The ECAP route C is chosen (180° rotation between each pass). The punch pushes the sample through the die at a constant speed of 10 mm/min. MoS_2 lubricant was used to reduce the friction between the sample and the channel surface, avoiding the samples getting stuck in the die.

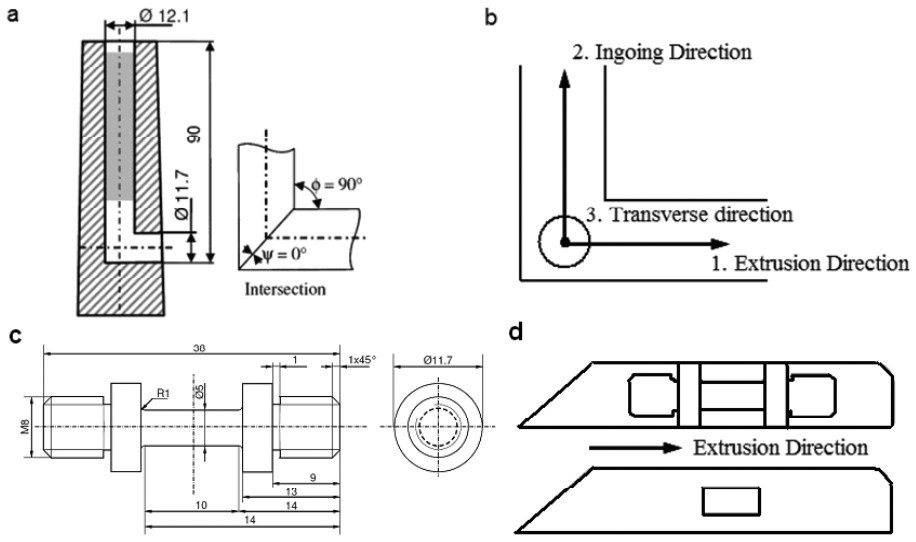

Fig. 1. A schematic of the ECAP die and the geometry of the specimen (a) the geometry of the ECAP die (b) the macroscopic reference frame of the die (c) the geometry of the tensile specimen (d) the position of the tensile/compression specimen with respect to the ECAP sample.

Table 1. The yield strength of the ECAP processed AA1050 samples, the estimated back-stress and the chemical composition of the material.

Pass	*Yield Strength* (MPa)		*Backstress* (MPa)
	Tensile	*Compression*	
Pass 1	141	82	29.5
Pass 2	160	94	33
Pass 3	167	88	39.5
Pass 4	179	84	47.5
Pass 8	194	82	56

Element	Fe	Si	Mn	Cu	Ti	other	Al
(wt.%)	0.32	0.12	<0.05	<0.05	<0.05	<0.05	Balance

2.2. Tensile tests and compression tests

The tensile specimens are machined from the homogenous part of the ECAP processed cylindrical samples. Their geometry is shown in Fig. 1c.

The tests were performed on a mechanical test machine INSTRON 4505. The speed of the cross-head is set to 5mm/min; the initial strain rate is equal to 8.33×10^{-3}/s.

It is known that ECAP produces ultrafine-grained (UFG) material. For these materials, flow localization in the sample neck is observed almost immediately after yielding. Segal proposed a geometrical method to recover the true stress-strain curve during the tensile test of UFG material [8]. This method is used in this work to obtain a true stress-strain curve from the force-displacement curve of the tensile tests.

The compression samples, with a diameter of 6 mm and a height of 9 mm, are cut from the middle part of the ECAP processed AA1050. The compression speed is set to 5 mm/min and the initial strain rate is equal to 9.26×10^{-3}/s. A polymer thin film was used as lubrication. The true stress-strain curve was converted from a force-displacement curve.

The yielding stress both of the tensile curves and the compression curves are determined by using the offset method with a small strain of 0.002. The results are shown in Table 1.

2.3. The back-stress and its estimation

In this work, the macroscopic back-stress σ_b is defined along the extrusion direction as a function of the yielding strength of the tensile test σ_{yt} and the compression test σ_{yc}:

$$\sigma_b = \frac{1}{2}\left(\sigma_{yt} - \sigma_{yc}\right). \quad (1)$$

The back-stress tensor **X** is described according to the reference frame in Fig. 1b. Therefore, the macroscopic back-stress σ_b is equal to the X_{11} component of **X.** The estimated back-stresses of aluminium AA1050 processed by ECAP route C along ED are shown in Table 1.

3. PREDICTION OF THE BACK-STRESS USING A PHENOMENOLOGICAL MODEL

3.1. Teodosiu and Hu's mixed hardening model

The model of Teodosiu and Hu, based on experimental observations [9,10] is a mixed (isotropic-kinematic) macroscopic phenomenological hardening law [3,4]. First developed for IF steels for moderate strains, it has been extended to aluminium [11]. Its flexibility is illustrated by the fact that it has been used for multi-phase materials like DP steels [4,12].

This hardening law adopts a set of four internal variables (R,**X**,**P**,**S**). R is a scalar variable and represents the isotropic hardening contributed from the statistically distributed dislocations. Its evolution is described by the equation

$$\dot{R} = C_R(R_{sat} - R)\dot{\lambda}, \quad (2)$$

where $\dot{\lambda}$ is the plastic multiplier, R_{sat} is the saturation value of R and C_R characterizes the rate of approaching the saturation.

The second-order dimensionless tensor **P** is associated with the polarity of the dislocation sheets. When the material is fully annealed, **P** should be

equal to zero. During plastic deformation, **P** polarizes along the current strain rate mode $\mathbf{N}=\mathbf{D}^p/||\mathbf{D}^p||$, $\mathbf{D}^p$ is the strain rate tensor. The following equation describes the saturation behaviour of **P**:

$$\overset{\circ}{\mathbf{P}} = C_p(\mathbf{N}-\mathbf{P})\dot{\lambda}, \tag{3}$$

where C_p controls the polarity rate.

The back-stress **X** represents the kinematic hardening part, which is associated with the motion of less stable dislocations, such as piled-up dislocations and the short-range interaction between dislocation and cell. For a fully annealed material, **X** is assumed to be equal to zero. During plastic deformation, its evolution is described as:

$$\overset{\circ}{\mathbf{X}} = C_X(X_{sat}\mathbf{N}-\mathbf{X})\dot{\lambda}, \tag{4}$$

where C_x represents the saturation rate of the back-stress. The scalar function X_{sat} is the saturation value of the back-stress, depending on the dislocation sheet evolution. Thanks to this tensor X, the evolution of the back-stress can be predicted and compared with the experimental results.

The evolution of dislocation sheets are described by the fourth-order tensor **S**, which consists of two parts, S_D and S_L:

$$\mathbf{S} = \mathbf{S}_L + S_D\mathbf{N}\otimes\mathbf{N}, \tag{5}$$

where the strength S_D is a scalar associated with the active slip systems. The strength $\boldsymbol{S}_L$ is a tensor associated to the latent part of the dislocation structures. Two evolution equations are adopted for them:

$$\dot{S}_D = C_{SD}\left[g(S_{sat}-S_D)-hS_D\right]\dot{\lambda} \tag{6}$$

and

$$\overset{\circ}{\mathbf{S}}_L = -C_{SL}\left(\frac{||\mathbf{S}_L||}{S_{sat}}\right)^{n_L}\mathbf{S}_L\dot{\lambda}, \tag{7}$$

where C_{SD} and C_{SL} control the saturation rate of S_D and $\mathbf{S}_L$ respectively, and S_{sat} is the saturation value of S_D. The scalar function *g* describes the work-hardening stagnation under reversed deformation and the scalar function *h* describes the micro-plastic stage. The term $\left(\frac{||\mathbf{S}_L||}{S_{sat}}\right)^{n_L}$ is introduced in order to take into account the effect of the pre-deformation on the subsequent hardening.

3.2. Texture prediction and yield locus

In its initial version described in [3], the Teodosiu-Hu's model was coupled with the Hill yield criterion. However Hiwatashi *et al.* [13] proposed to associate it with a series function describing the yield locus identified through the use of the Taylor polycrystal plastic model applied on the measured texture. In a similar way, the so called MINTY model from Duchêne and Habraken will be used in the present work to predict the mechanical behaviour and update the texture [14]. Instead of obtaining an analytical expression of the whole yield surface, the MINTY model uses a stress-strain interpolation method to describe a local yield surface in the 5-dimensional stress space and the 5-dimensional strain rate space. It established a local interpolation zone, constructed through five neighbouring points, by calling the Taylor-type polycrystal plastic model only five times. It saves a lot of computation time with negligible error compared to the conventional Taylor model.

3.3. Material parameters

The Teodosiu and Hu's model needs to identify thirteen material parameters from a series of mechanical tests, namely uniaxial tensile test, plane strain test, simple shear test, Bauschinger test and orthogonal test. It is assumed that the deformation mode of ECAP route C is just a combination of forward and reversal simple shear in the shear plane [1]. Based on this assumption, the identification procedure can be reduced. Only eight out of the thirteen parameters, which are in charge of the reversal strain path change, need to be identified. The identified parameters are shown in Table 2.

3.4. Numerical results

The non-linear finite element software LAGAMINE, developed by the University of Liège, is used here

Table 2. The eight material parameters of Teodosiu-Hu hardening model identified from the experiments.

Parameter	C_p	C_{sd}	C_x	X_{sat} (MPa)	f	S_{sat} (MPa)	R_o (MPa)	C_R	R_{sat} (MPa)
Value	1.59	5.63	55	5.29	0.85	55	50	77.1	20

to perform a one-element simulation to model the 8 passes of the ECAP route C processing. The Teodosiu and Hu's hardening model coupled with the MINTY model is chosen, to model mechanical behaviour and texture evolution. The predicted back-stresses of the pure aluminium after each ECAP pass are shown in Fig. 2. The Teodosiu-Hu model predicts the back-stress fluctuating around 10MPa, lower in the odd passes and higher in the even passes. Compared to the experimental values, the back-stresses are largely underestimated by about 20~30 MPa even after one pass. In [11] the strain gradient plasticity model developed by Evers [15] was also applied on this process. Fig. 2 gives the improved predicted result. Even if the prediction level was better than with the Teodosiu-Hu model, this approach also lacks to assess the experimental evolution of the component X_{11} of the back-stress tensor where no oscillation between even and odd passes happens.

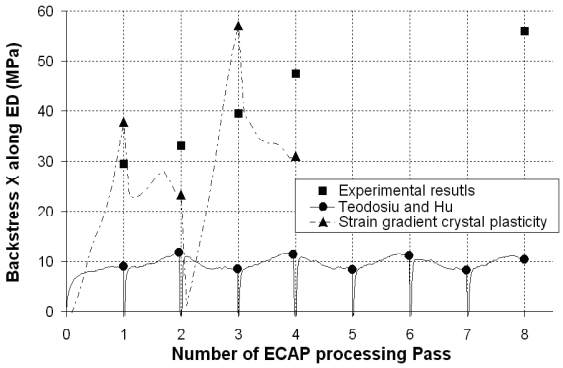

Fig. 2. Back-stresses along the extrusion direction are compared: from the experiment, predicted from the Teodosiu-Hu model and from a strain gradient crystal plasticity model in [13].

4. PREDICTION OF THE BACK-STRESS USING A DISLOCATION-BASED MODEL

4.1. Estrin-Tóth dislocation-cell model

The microscopic dislocation-based model from Y. Estrin and L.S. Tóth is able to describe the hardening behaviour of a cell-forming crystalline material at large strain [5]. So far, this model has been improved by taking into account the fragmentation of grains, e.g. the model from I.V. Alexandrov and R.G. Chembarisova [20], and the new model from L.S. Tóth and Y. Estrin themselves [21]. For simplicity, the conventional Estrin- Tóth is used in this work.

This model adopts the idea of describing the flow stress of a material containing a cell structure by the rule of mixture:

$$\tau = f\tau_w + (1-f)\tau_c , \tag{8}$$

where f is the volume fraction of the cell wall, τ_w represents the flow stress of the cell wall and τ_c describes the flow stress of the cell interior. Based on the work of Kocks and Mecking [16], these two flow stress components are described in a strain rate sensitivity equation:

$$\tau_w = \alpha Gb\sqrt{\rho_w}\left(\frac{\dot{\gamma}_w^r}{\dot{\gamma}_0}\right)^{1/m},$$
$$\tau_c = \alpha Gb\sqrt{\rho_c}\left(\frac{\dot{\gamma}_c^r}{\dot{\gamma}_0}\right)^{1/m}, \tag{9}$$

where $\dot{\gamma}_w^r$ denote the strain rate in the cell walls, by analogy with that in the cell interiors, $\dot{\gamma}_c^r$; the term 1/m is the strain rate sensitivity index, $\dot{\gamma}_0$ is a reference shear rate; *a* is a material parameter, *G* is the shear modulus and *b* is the magnitude of the Burgers vector; ρ_c and ρ_w are the dislocation density of the cell interior and the one of the cell wall. Their evolution law can be described by the two following equations:

$$\dot{\rho}_c = \alpha^* \frac{1}{\sqrt{3}}\frac{\sqrt{\rho_w}}{b}\dot{\gamma}_w - \beta^* \frac{6\dot{\gamma}_c}{bd(1-f)^{\frac{1}{3}}} - k_0\left(\frac{\dot{\gamma}_c}{\dot{\gamma}_0}\right)^{-\frac{1}{n}}\dot{\gamma}_c\rho_c ,$$
$$\dot{\rho}_w = \frac{\sqrt{3}\beta^*\dot{\gamma}_c(1-f)\sqrt{\rho_w}}{fb} + \frac{6\beta^*\dot{\gamma}_c(1-f)^{\frac{2}{3}}}{bdf} - k_0\left(\frac{\dot{\gamma}_w}{\dot{\gamma}_0}\right)^{-\frac{1}{n}}\dot{\gamma}_w\rho_w , \tag{10}$$

where the α^* and β^* are geometrical parameters and *n* is inversely proportional to the absolute temperature. Both these two evolution equations contain three terms, which contributes from different dislocation mechanisms. The first mechanism is the creation of dislocations in the cell interior. The second one comes from the dislocation motion, moving from cell interior to cell wall or from cell wall to cell interior. The last part is given by the mutual annihilation of dislocations with opposite sign.

Once the dislocation densities of the cell wall and of the cell interior are known, the total dislocation density can be calculated:

$$\rho_l = f\rho_w + (1-f)\rho_i , \tag{11}$$

and the average cell size d is linked with the total dislocation density:

$$d = \frac{K}{\sqrt{\rho_i}} , \tag{12}$$

where K is a proportionality constant. These two evolutions show how the model takes the average cell size into account. The most interesting idea of Estrin and Tóth's model is that it introduces an evolution law of the volume fraction f in order to describe the growth of the cell size. The evolution law is expressed in an exponential way:

$$f = f_\infty + (f_0 - f_\infty)\exp\left(\frac{-\gamma^r}{\tilde{\gamma}^r}\right), \tag{13}$$

where f_0 is the initial value of the volume fraction of cell walls, f_∞ is its saturation value at large strains. The quantity $\tilde{\gamma}^r$ describes the rate of variation of ¦ with resolved shear strain γ^r.

For simplicity, Estrin and Tóth assumed that all the dislocation cells within a grain are identical. In this way, a unique resolved shear strain rate is prescribed to describe the same response of these cells to the external force.

$$\dot{\gamma}^r = \left[\sum_{s=1}^{N} \dot{\gamma}_s^{\,r\frac{m+1}{m}}\right]^{\frac{m}{1+m}} , \tag{14}$$

where N defines the total number of the active slip systems and $\dot{\gamma}_s^r$ the shear rate on the slip system s.

The material parameters for the pure aluminium are taken from the work of Baik *et al.* [17]. The material is prescribed as fully annealed, the initial dislocation density is chosen as $1x10^8$ m^{-2} both in the cell wall and the cell interior. The model parameters and their value are summarized in Table 3.

4.2. Sauzay's intragranular back-stress model

The intragranular back-stress, induced by the dislocation cell-and-wall structures, is able to be predicted by an analytical model proposed by Sauzay [6]:

$$X = -\frac{f}{1-f} G(1-\beta) F_{accom} \sum_{i=1}^{N} \gamma_i^p \left(n_i m_i^T + m_i n_i^T\right), \tag{15}$$

where f is the volume fraction of the cell wall, n_i and m_i defines the current active slip system i, and β is a scalar function of the Poisson coefficient. In this work, the plastic accommodation factor is prescribed as:

$$F_{accom} = \left(1 + \frac{1}{2}\mu\frac{\varepsilon_{eq}^p}{\sigma_{eq}}\right)^{-1} . \tag{16}$$

This factor assumes that the back-stress tensor is no longer a linear relation of the plastic strain once the strain is large enough.

4.3. Yield criterion and texture

Considering the effect of the back-stress, a kinematic type yielding criterion in a macroscopic scale is defined:

$$F = R - X , \tag{17}$$

where R is the macroscopic stress given by the Full-constraint Taylor model with the critical resolved shear stress in equation and X represents the kinematic hardening part using Eq.(8). The FC Taylor model coupled with the Estrin-Tóth's dislocation-cell model and the Sauzay's intragranular back-stress model defines the whole constitutive law.

Table 3. The material parameters for the Estrin and Tyth's dislocation-cell model [17].

Materialparameters	$\rho_w^{t=0}$ (m^{-2})	$\rho_c^{t=0}$ (m^{-2})	f_0	f_∞	$\tilde{\gamma}^r$	$\dot{\gamma}^r$	m	n
value	$1x10^8$	$1x10^8$	0.25	0.06	3.2	1.0	100	67

Materialparameters	α	G (GPa)	b (m)	K	α*	β*	k_0
value	0.25	26.3	$2.86x10^{-10}$	30	0.0024	0.0054	3.22

4.4. Model implementation and theoretic prediction

The whole model is implemented using Intel Visual Fortran. The IMSL numerical library is used to solve two mathematical problems. On one hand, the subroutine DLPRS (revised simplex method) is called to solve the linear programming problem in Taylor single crystal plasticity model. On the other hand, the subroutine IVPAG (Adams-Moulton's method) is called to solve the initial-value problem for the dislocation evolution equations of the Estrin-Tyth model (ordinary differential equations).

The model simulates the ECAP deformation of one central material point until the equivalent strain is equal to 1.15 (one single pass). This strain is achieved by 100 simulation steps and for each step the velocity gradient tensor L is expressed in the coordinate system in Fig. 1b:

$$L = \begin{bmatrix} 0.01 & -0.01 & 0 \\ 0.01 & -0.01 & 0 \\ 0 & 0 & 0 \end{bmatrix}. \qquad (18)$$

The theoretic predictions are shown in Fig. 3.

In Fig. 3a, the average cell size quickly decreases at the beginning of the simulation and tends to evolve more slowly at large strain. After one ECAP pass, the cell size is predicted as 1.33 μm, which is very close to the EBSD measured size in previous work [18]. The dislocation density in the cell wall evolves in an exponential way and ends at 3.35×10^{15} m^{-2} (Fig. 3b). Meanwhile the dislocations in the cell interior slowly propagate to the density of 8.08×10^{13} m^{-2}, consequently resulting in the average dislocation density of 5.14×10^{14} m^{-2}.

Fig. 3c shows the evolution of the accommodation factor F_{accom} for a random orientation. Starting from a quasi-linear relationship with the strain, this factor quickly reaches saturation and falls back. The most important result is shown in Fig. 3d. The back-stress along the extrusion direction after one pass is predicted as 26.7 MPa. Compared to the experimental value, this model is believed to be capable of predicting the back-stress actually.

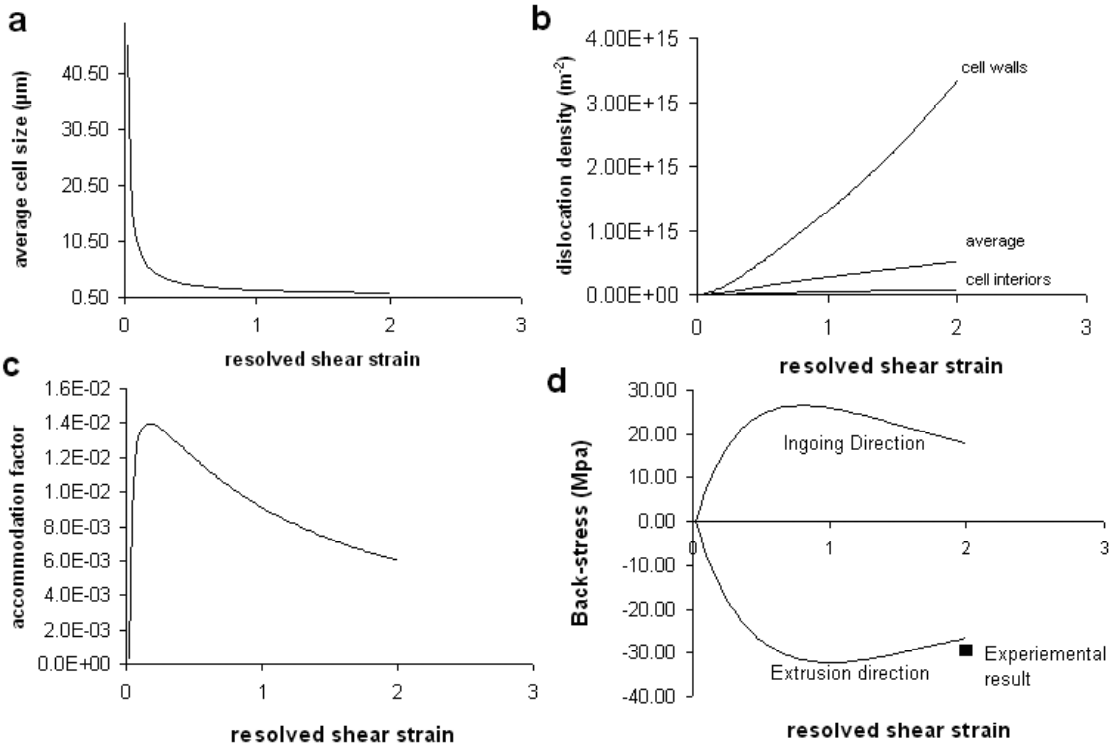

Fig. 3. Theoretic prediction from the present new model (a) the evolution of the average cell size (b) the dislocation density in cell walls and cell interiors (c) the accommodation factor of a random orientation (d) the predicted back-stress compared with the experimental result.

5. DISCUSSION

Based on the simulation results, it is clear that for one pass ECAP process the proposed dislocation-based mixed-hardening model gives a better prediction of the back-stress than the phenomenological Teodosiu-Hu hardening model.

The Teodosiu-Hu model underestimated the back-stress level. It even predicted that the back-stress did not essentially increase after multiple ECAP passes. The ideal deformation mode of the ECAP route C is a combination of forward and reversal simple shear on the same shear plane. According to this assumption, the predicted fluctuating back-stress after odd and even passes only reflects the different polarity level of the microstructure. In fact, there is no possibility within the Teodosiu-Hu model to model the decreased cell size and the Hall-Petch relationship. It is a main drawback as the sub-grain size will dominate the strength of the material once the dislocation-cell substructures form. According to the literature, the Teodosiu-Hu model is proposed based on the experimental observation of persistent dislocation sheets, which means this model should be able to predict the hardening phenomenon up to the moderate strain. However, pure aluminium is a typical cell-forming material. Once the dislocations evolved into cell structures, the polarity of these dislocations disappears at the macroscopic scale.

On the other hand, the proposed dislocation-based mixed-hardening model seems to work fine for the prediction of the single pass ECAP aluminium. It generally overcomes the drawbacks of the Teodosiu-Hu model. The Estrin-Tóth model captures the evolution of the cell microstructure. The predicted cell size is very close to the measured one. In this way, the hardening contribution from the Hall-Petch relation is taken into account. This is the first reason why the proposed model is able to predict the back-stress. Secondly, the predicted average dislocation densities, as well as their ratio between the cell walls and cell interiors are in reasonable agreement with experiments [19]. This composite microstructure of different dislocation densities in both regions is the essential source of the induced back-stress. Besides, the Estrin-Tóth model predicts the evolution of the volume fraction of cell walls. This is an important aspect of the proposed model. It is the evolved volume fraction that allows the Sauzay's equation to estimate the back-stress level.

The accommodation factor also plays a role (see Fig. 3c). The evolution of this value can be divided into two parts. The first part starts from the beginning of the deformation and ends at the resolved shear strain of 0.1. The quickly increased accommodation factor implies a linear relationship between the back-stress and the accumulated resolved shear. Note that it is assumed that the starting dislocation densities are the same in cell walls and cell interiors. In this part, the cell-and-wall microstructure hasn't developed well. The polarity of the dislocations and the propagation of the dislocations contribute to the back-stress. During the second evolution part of the accommodation factor, the piled up dislocations form the cell-and-wall structure. The polarity level of the dislocation microstructures is decreasing. The energy associated with the dislocation polarity is released by forming the cell-and-wall microstructure. Therefore, the induced back-stress should be determined by the large difference of dislocation densities in cell walls and cell interiors. The physical meaning of the accommodation factor should be clarified by further experimental work.

6. CONCLUSION

In the present work, two models at different length scales are used to model the back-stress level of ECAP processed pure aluminium. The back-stress is experimentally measured. A new dislocation-based mixed-hardening model is proposed, based on the Estrin-Tyth dislocation model and the Sauzay's back-stress model. From the results obtained, the following conclusions can be drawn:

- The back-stress of the ECAP route C processed pure aluminium increases after each pass, from 29.5 MPa for pass one to 56 MPa for pass eight.
- The Teodosiu-Hu hardening model largely underestimated the back-stress of the ECAP processed aluminium. It is believed to be due to the fact that no sub-grain size evolution is considered within this model.
- The present model predicts the back-stress of one pass pure aluminium very well. The model overcomes the drawbacks of the Teodosiu-Hu hardening model by capturing the cell evolution, modelling the composite microstructure and introducing the accommodation factor.

ACKNOWLEDGEMENTS

The authors acknowledge the financial support from the 'Interuniversity Attraction Poles Programme – Belgian State–Belgian Science Policy (Contract P6/24)'. L.D. and A.M.H. also acknowledge the Belgian Fund for Scientific Research FRS-FNRS.

REFERENCES

[1] R.Z. Valiev and T.G. Langdon // *Progress in Materials Science* **51** (2006) 881.
[2] S. Poortmans and B. Verlinden // *Materials Science Forum* **503-504** (2006) 847.
[3] C. Teodosiu and Z. Hu, *Proceedings of the NUMIFORM'95* (Balkema, Rotterdam, 1995).
[4] H. Haddadi, S. Bouvier, M. Banu, C. Maier and C. Teodosiu // *International Journal of Plasticity* **22** (2006) 2226.
[5] Y. Estrin, L. S. Tóth, A. Molinari and Y. Brechet // *Acta Materialia* **46** (1998) 5509.
[6] M. Sauzay // *International Journal of Plasticity* **24** (2008) 727.
[7] Y. Iwahashi, J. Wang, Z Horita, M. Nemoto and T.G. Langdon // *Scripta mater* **35** (1996) 143.
[8] V.M. Segal, S. Ferrasse and F. Alford // *Mater. Sci. Eng. A* **422** (2006) 321.
[9] E.F. Rauch and J.-H. Schmitt // *Mater. Sci. Eng. A* **113** (1989) 441.
[10] X. Huang // *Scripta Mater.* **38** (1998) 1697.
[11] L. Duchêne, M.G.D. Geers, W.A.M. Brekelmans, E. Chen, B. Verlinden and A.M. Habraken, In: Proc. *ICOTOM 15* (Ceramic Transactions, vol. 200, Pittsburgh, PA, 2008), p. 671.
[12] B. Gardey, S. Bouvier, V. Richard and B. Bacroix // *Materials Science and Engineering A* **400-401** (2005) 136.
[13] S. Hiwatashi, A. Van Bael, P. Van Houtte and C. Teodosiu // *Computational Materials Science* **9** (1997) 274.
[14] A.M. Habraken and L. Duchêne // *International Journal of Plasticity* **20** (2004) 1525.
[15] L.P. Evers, W.A.M. Brekelmans and M.G.D. Geers // *International Journal of solids and structures* **41** (2004) 5209.
[16] U. F. Kocks and H. Mecking // *Progress in Materials Science* **48** (2003) 171.
[17] S.C. Baik, Y. Estrin, H.S. Kim and R.J. Hellmig // *Mater. Sci. Eng. A* **351** (2007) 86.
[18] S. Poortmans, L. Duchêne, A.M. Habraken and B. Verlinden // *Acta Materialia* **57** (2009) 1821.
[19] L.S. Tóth, A. Molinari and Y. Estrin // *J. Eng. Mater. Technol.* **124** (2002) 71.
[20] I.V. Alexandrov and R.G. Chembarisova // *Rev. Adv. Mater. Sci.* **16** (2007) 51.
[21] L.S. Tóth, Y. Estrin, R. lapovok and C.F. Gu // *Acta Materialia* **58** (2010) 1782.